This article has been accepted for publication in IEEE Transactions on NanoBioscience. This is the author's version which has not been fully edited and content may change prior to final publication. Citation information: DOI 10.1109/TNB.2022.3202242



# Temperature Imposed Sensitivity Issues of Hetero-TFET Based pH Sensor

Amit Bhattacharyya, Debashis De, *Senior Member, IEEE*, Manash Chanda, *Senior Member, IEEE*

***Abstract*—An underlapped hetero-structure electrolyte Bio-TFET for potential of hydrogen (pH) sensing has been presented in this article. Intersection charge density ($D_{it}$) near the substrate-oxide junction can be employed to represent pH value within the simulation. A feasible fabrication scheme for the proposed model is specified here. A detailed simulation is performed with an ATLAS device simulator to examine the efficiency of the projected sensor. The impact of pH alterations on device features akin to the drain current ($I_{DS}$), threshold potential ($V_{TH}$), sensitivity regarding voltage ($S_V$), and current ($S_I$) is examined. The effect of phosphate-buffered saline (PBS) concentrations on the pH buffer are also scrutinized. Moreover, the impact of the reference voltage and current ($V_{Ref}$ and $I_{Ref}$), and channel doping concentration ($N_{CH}$) over $S_V$ and $S_I$ is analyzed methodically. Here, $S_V$ attains ≈ 100 mV/pH, which is superior to the Nernstian limit (59 mV/pH) and $S_I$ enhances nearly ten times per pH variation. Benchmarking is included to provide a quantitative assessment of the proposed model with the published literature. The impact of temperature on pH buffer, $I_{DS}$, temporal drift parameters and sensitivities have been emphasized. Finally, the temperature-immunity aspect of the proposed Bio-HTFET based pH sensor is highlighted by comparing sensitivity parameter among state-of-the-art literature. Hence, the recommended pH sensor can be utilized as an outstanding substitute for the succeeding generation of biosensor applications.**

***Index Terms*— Tunnel FET, hetero-structure, electrolyte, pH sensor, Nernstian limit, temperature and temporal drift, sensitivity.**

## I. Introduction

IN Ion-sensitive field-effect transistors (ISFETs), variation of surface potential (ψ) with respect to the pH of an aqueous solution is a pivotal issue in determining the sensitivity of the sensor [1]-[4].

A plethora of ISFET has been reported in literature. These mainly highlight experimental process [2], analytical modeling [1] and simulations [3], [4] to obtain better sensitivity than the Nernstian limit (≈ 59.2 mV/pH at 300 K). However, none of them addressed the impact of temperature on the sensitivities of the pH sensors. Temperature can variegate mobility of the electrons or holes of the FET structure. The pH of hydrogen ion buffer changes with temperature also. Increase in temperature impels the molecular vibrations, so, the amount of the recognizable [H+] also enhances with temperature [5]-[6]. Furthermore, temperature increase brings down the pH sensitivity, i.e. $S_{pH}$ (ΔpH/ΔT), the electrolyte-oxide interface charges and surface dipole potential of the solvent are swayed by the temperature variations. So, the sensitivity of the ISFET is susceptible to temperature variations and must be addressed properly in the literature.

Fig. 1(a)-(b) delineates the variation of equivalent ψ in an electrolyte (e)-insulator (i)-semiconductor (s) (EIS) structure following the Gouy-Chapman-Stern (GCS) hypothesis [3]-[6]. Here, IHP and OHP: inner and outer Helmholtz plane; $\psi_D$, $\psi_{e\text{-}i}$, $\psi_{s\text{-}i}$ and $V_{Ref}$: the potentials at the boundary of diffuse layer, e-i junction, s-i intersection, and the reference electrode. Dwivedi *et al.* [4] and Kim *et al.* [7] proposed underlap TFET for pH sensing, showing better sensitivity without gate electrode. Although the estimated sensitivity values [4], [7] are impractical as impact of temperature has not been considered here.

In this article, an electrolyte biosensor based on n-type underlapping hetero-junction TFET (HTFET) has been proposed to attain the sensitivity superior to the Nernstian limit. Here, an underlapped Bio-TFET [7]-[9] configuration is employed owing to (i) more sensing surface areas (ii) extremely CMOS compatibility (iii) surmount the hindrance for incorporating reference electrode on-chip in ISFET (iv) more hybridization of bioanalytes as no gate-electrode (v) assist tunneling of carriers in the solvent. Hence, the proposed model improves the sensitivity, superior to 59.2 mV/pH. Here, to improve $I_{ON}$ and steeper SS, a HTFET is preferred [10]-[11].

The novelty of this work is to investigate the impact of temperature on pH sensitivity. Optimization of Bio-HTFET for better sensitivity; investigation of the device performances; analysis of the $S_{pH}$ (ΔpH/ΔT); pointing out the temperature-immunity feature of proposed pH sensor by comparing with the state-of-the-art literature are also detailed here.

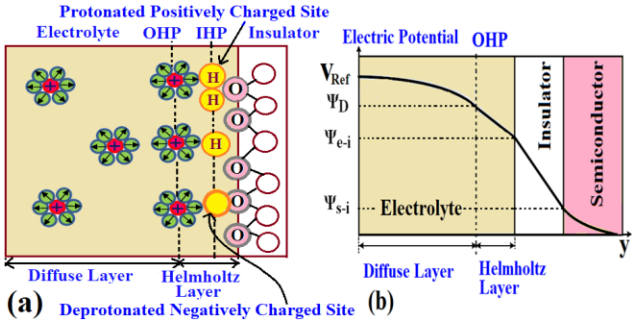


Fig. 1.Schematic of site-binding (SB) and the electric double layer (EDL) at EIS structure and (b) Equivalent potential allotment in an EIS model.

## II. Device Structure And Functionalization

The cross sectional outlook of a n-type underlap electrolyte Bio-HTFET is shown in Fig. 2(a).Target bio-analytes inside the electrolyte are gathered near the underlap section. To perceive the pH of electrolyte, n-TFET with $T_{si}$ = 10 nm [8]-

A. Bhattacharyya is with the Dept. of ECE, Haldia Institute of Technology, Haldia, West Bengal, India (e-mail: amit_elec06@yahoo.com).

D. De is with the Dept. of CSE, Maulana Abul Kalam Azad University of Technology, Kolkata, 700064, India (e-mail:dr.debashis.de@gmail.com).

M. Chanda is with the Dept. of ECE, Meghnad Saha Institute of Technology, Kolkata, 700150, India (e-mail:manash.bst@gmail.com).

This article has been accepted for publication in IEEE Transactions on NanoBioscience. This is the author's version which has not been fully edited and content may change prior to final publication. Citation information: DOI 10.1109/TNB.2022.3202242



[11], (<Debye length [8], [11]), since for $T_{Si}$< 10 nm, quantum mechanical effect (QME) [8], [11] turns into severe. Besides, front gate (FG) length ($L_{FG}$) = 200 nm, length of underlap ($L_{un}$) region = 50 nm near the source side, height of FG dielectric ($T_{ox1}$) = 40 nm and height of buried dielectric ($T_{Box}$) =10 nm, Gate width ($W_G$) = 1 µm, FG work-function ($\varphi_{FG}$) = 4.2 eV [12] is utilized in the configuration. The stern film [3] thickness ($T_{Stern}$) = 1 nm, and its dielectric constant ($\varepsilon_{Stern}$) =2.25$\varepsilon_0$ is assumed. Thiol-linker with $\varepsilon_{linker}$ = 32$\varepsilon_0$ [13] and height = 2 nm is employed as silica binding protein.

Compared to Silicon dioxide ($SiO_2$), Aluminum oxide ($Al_2O_3$) has more efficient resistivity to hydration [14], hence $Al_2O_3$ might be a better option as a dielectric layer in pH sensor. However, the functionalization of the surface is extremely vital to assure suitable transduction in biosensors through organized binding of bioanalytes [15]. In rigid attaching, functionality of the surface declines [16]. Conversely, bioanalytes adsorption on $SiO_2$ layer relies upon (1) surface adaptation to attach particular functional species (2) covalently affection of cross-linkers [15] (3) fixing of bioanalytes covalently [16]. 3-aminopropyltrietho-xysilane (APTES) and 3-glycidoxypro-pyltrimethoxysilane (GOPS) are two supreme protocols for proteins, enzymes and ssDNA adsorption [15]-[16]. GOPS procedure involves (i) Surface cleaning via oxidation (ii) stimulation of Hydroxyl group (OH-) (iii) silanization through GOPS (iv) deposition along with DNA oligonucleotides fixation and (v) ssDNA immobilization through $NH_2$ (amino group) abolishing. GOPS procedure for adsorption of ssDNA is illustrated in [16]. It has been reported that the $SiO_2$ layer with covalent linkage can increase the biomolecule's interaction [7]. Besides, Silica has immense chemical stability [15]. Moreover, the balanced bindings, and structural consistency throughout biological processes are essential aspects of $SiO_2$. Hence, a 4 nm thin $SiO_2$ layer is formed on the underlap region to enhance the immobilization of bioanalytes [4], [7].

Vroman effect [17] reveals that adsorption of biomolecules will alter relying on the binding potency and affinity of surface too. Because of a variety of amino acid compositions within the proteins, intermolecular force (IMF) alters the isoelectric points (pIs), conformations and spherical shapes, i.e., globular protein symmetricity and asymmetrical for the extended or Y-formed proteins likely immunoglobulin-G (IgG) [16]. Hence, alongside pIs, globular shapes and the composite organization of the proteins influence the adsorption procedure as well. Physico-chemical parameters akin to pH, ionic potency, surface chemical reactions, buffer configurations, temperature etc. are liable for protein adsorption procedures owing to their weak binding and mostly persuade the rate of adsorption and the stability state of adsorption method also [15]-[16]. These also affect the incubation time and the process. The deviation of pH of a solution is associated with the ionic molarity [16]. Ionic potency deviation infects the adsorption probability and charged protein kinematics. The net amount of absorbed proteins on the surface enhances while temperature rises, and influence the equilibrium state firmly [16]. Besides, to achieve a reasonable limit of detection (LOD) [16], sufficient number of biomolecules should be incubated [18] over a large sensing surface. Sometimes, this might be challenging if the diagnostic samples are obtained from the human body and valuable. Occasionally, the gate voltage varies significantly with the incubation time, which also affects **$S_I$** [18]. In brief, the incubation time for the interaction of capture probes and target molecules should be optimized considering the LOD [16]. Conversely, the equilibrium state associated with the bioanalyte concentration might be estimated by the equilibrium approach specified in [16]. Thus, assuming a suspension of sphere-formed proteins having distinct dimension with charge inside a solution, through noting the free-energy of the procedure concerning molar concentration, equilibrium hypothesis is achieved [16].

Contrasted to $SiO_2$, silicon nitride ($Si_3N_4$) has a much superior diffusion resistivity to water and sodium [19]. Besides, the proton ion ($H^+$) diffusivity of $SiO_2$ ($3.3 \times 10^{-16}$ $cm^2$/sec) is significantly greater than those of $Si_3N_4$ ($10^{-19}$ $cm^2$/sec) [19]. Moreover, $Si_3N_4$ directs enormously chemical stability with an outstanding barrier feature. Hence, $Si_3N_4$ is used as a passivation layer to evade source and drain contact with electrolyte [4]. Asymmetric source doping ($N_S$) of $2\times10^{20}$ $cm^{-3}$, and drain doping ($N_D$) of $5\times10^{18}$ $cm^{-3}$ together with overlapping of $Si_3N_4$ of 20 nm to the drain/channel intersection is utilized to control the ambipolar activities [12].

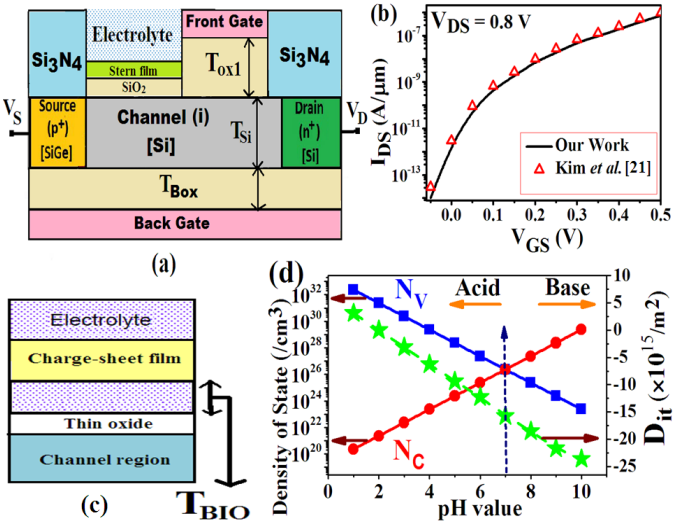


Fig. 2. (a) Schematic diagram of a n-type underlapped ionic Bio-HTFET (b) Model validation with the experimental data in [21] (c) Target biomolecules location ($T_{BIO}$) =0 nm, 2 nm, 5 nm among CS film and thin oxide (d) Variation of DoS ($N_C$ and $N_V$) of undoped semiconductor and $D_{it}$ regarding pH value.

## III. Simulation Set-up

The simulation is executed with the help of commercially available Silvaco ATLAS device simulator [20], V5.19.20. Tunneling event in TFET is confined through nonlocal band-to-band tunneling (BTBT) model recommended by Kane together with models of field-dependent and concentration-dependent mobility, Shockley–Read–Hall (SRH) method, bandgap narrowing, and Fermi Dirac statistics to examine the arrangements. To authenticate and normalize this process and models, the simulation outcome is calibrated with Kim *et al.* [21], which is exhibited in Fig. 2(b). In Silvaco ATLAS, the nonlocal BTBT model is based on an implemented model by Silvaco. It is based on fitting electron and hole tunneling masses. Instead, Kane model, implemented in Silvaco, is a

local model. Here, BTBT ($A_{Kane}$= $3.4\times10^{21}$ $eV^{0.5}/cm–s\text{-}V^2$ and $B_{Kane}$= 22.4 MV/cm-$eV^{1.5}$; tunneling reliant factors); additional default values similar to me.tunnel= $0.322m_0$ Kg, mh.tunnel= $0.547m_0$ Kg, and NSRHN = NSRHP = $5x10^{16}/cm^3$ [20] have been chosen to achieve excellent similarity among the simulated and experimental results. The validation has been executed in a system, including a source of Ge, as practical verification over the $Si_{1-x}Ge_x$ TFET correlated to line tunneling is not obtainable. Fig. 2(b) presents a justification for the calibrated version, in which the device configuration, along with its measurements and design factors, has retained the identical, as employed in [21]. Since, during calibration purpose the simulation environment should be identical to [21], hence, the biasing potential has been set as, $V_{DS}$ = 0.8 V [10], throughout simulation. Moreover, the sub-threshold (sub-$V_{TH}$) zone has been favoured to obtain optimal sensitivity and better signal-to-noise ratio (SNR) [22]. A superb conformity among the simulated and detailed experimental results has been examined in Fig. 2(b).

The simulation environment has been set up by the following [1], [3]. In an actual ionic solvent, the allocation of charge is signified by the Poisson–Boltzmann equation (PBE). The thermally produced mobile carriers of semiconductor are exhibited by cations and anions of the solvent (1 mmol/L of NaCl), with the highest esteems of the mobilities ($\mu_{p,max}$) = $4.99\times10^{-4}$ $cm^2/V.S$ and ($\mu_{n,max}$) = $6.89\times10^{-4}$ $cm^2/V.S$ has been utilized to imitate the activities of $Na^+$ ions and $Cl^-$ ions, correspondingly [4]. In ATLAS simulation, the EDL has also been introduced [4] by assuming the underlap section consists of a 4 nm wide oxide layer with a relative permittivity of $2.25\varepsilon_0$ (bio-analyte membrane). All the profiles are extracted at a distance of 0.5 nm under the oxide/Si intersection.

Platinum (Pt) or Gold (Ag) reference electrode can be employed to realize the liquid gate [23]. Conversely, $SiO_2$ functionalization regions for recognition of various kinds of bioanalytes can be characterized via microfluidic channel. The reference electrode is fixed to Polydimethylsiloxane (PDMS) microfluidic channel in support of liquid gate [23]. This microfluidic channel is structured so that the fluids don't touch the source and drain ends, which is further ascertained via $Si_3N_4$ passivation sheet that does not protect the functionalization region. Hence, liquid gate remains stable.

- **SOI 10 nm BOX through oxidation and wet-etching using BOE**
- **MESA pattern formation through photolithography**
- **SAG of $Si_{1-x}Ge_x$ on source side of Si-film**
- **Masking and Ion-Implantation by $BF_2$ for source formation**
- **Masking and Ion-Implantation by P for drain formation**
- **Source/drain implants activation by RTA at 1000 $^0$C for 30 s**
- **40 nm thick front gate $SiO_2$ film deposition by thermal oxidation**
- **Deposition of p-type polycrystalline film and patterned to form 200 nm gate electrode**
- **$SiO_2$ etching to form underlap length near source/drain-gate**
- **4 nm thick $SiO_2$ deposition on the underlap area in source side through thermal oxidation**
- **Reservoir formation for pH buffer at the exposed gate window using PDMS by immersing in reversed osmosis water for 12 hours**
- **$Si_3N_4$ passivation layer deposition and patterning among source/drain with electrolyte area**
- **Contact formation and sintering through $H_2$**

Fig. 3. Fabrication flow for the proposed configuration.

The selected bio-analytes have been simulated similar to charge-sheet (CS) film as exposed in the Fig. 2(c). Here, target biomolecules location ($T_{BIO}$) = 0 nm (in an adjacent position) is assumed rather than $T_{BIO}$ = 2 nm, and 5 nm as $I_{DS}$ shifts towards the right side and hence $V_{TH}$ rises when $T_{BIO}$ changes from 0 nm to 5 nm [24]. This is due to position of CS film lying outside the Debye's screening length [24]. APTES bioanalyte ($\epsilon$ = 3.54) of charge density ($N_{APTES}$) ≈ -3 × $10^{12}/cm^2$ is contemplated in 1 × PBS (phosphate-buffered saline) solvent with pH = 7 rather than 0.1 × PBS and 0.01 × PBS since double layer capacitance ($C_{DL}$) is larger, and the voltage drop is lesser for 1 × PBS concentration [24]. Hence, it is examined that the $I_{DS}$ shifts towards the left side and thus $V_{TH}$ diminishes as the PBS solvent concentrations rises [24].

### *A. pH Evaluation*

The ionic concentration inside the electrolyte solvent, is expressed as, $n_E = N_V = N_C = N_{Avo}i_E \times10^{-3}$, where, $N_{Avo}$ = $6.023 \times 10^{23}$/mol and $i_E$ the ionic molarity (1 Molar = 1000 $mol/m^3$) inside the bulk region of the ionic solution. Hence, $N_C = 2[2\pi m_e^* K_B T/h^2]^{3/2}$ and $N_V = 2[2\pi m_h^* K_B T/h^2]^{3/2}$) represent the density of states; h, $m_e^*$, $m_h^*$are the Planck's constant, electron and hole effective mass respectively. Now, pH = -log (ionic molarity) = -log [$i_E$]. Hence, pH is given as: pH = -log($(N_V\times10^3)/N_{Avo}$) = - log($(n_E\times10^3)/N_{Avo}$) and pOH = -log($(N_C\times10^3)/N_{Avo}$). Here, pH + pOH = 14 (at 300 K). Fig. 2(d) depicts the variation of DoS ($N_C$ and $N_V$) of undoped SC material with pH value.

### *B. Potential Near Oxide-Electrolyte Interface (ψ)*

Ψ depends on the pH of the ionic solution and is expressed as [25]:

$$\psi = -\log_e 10 \times \eta \times V_T \times (pH - pH_{PZC}) \quad (1)$$

Where η = α / (1+ α) and α is evaluated by GCS model as: α = $qQ_S\gamma/(C_{eff}\times V_T)$; where $\gamma = 2\times10^{(pKa-pKb)/2}$ and $C_{eff}$ = ($C_{GCL}\times C_{STERN}$)/ ($C_{GCL}$+ $C_{STERN}$). Now, $pK_a = -\log_{10}(K_a)$ and $pK_b = -\log_{10}(K_b)$, where, $K_a$ and $K_b$ denote acid and base ionization constant for the surface respectively [4]. Here, $C_{STERN}$ denotes capacitance of the stern film and is 20 $\mu F.cm^{-2}$ [1], [3]-[4], and $C_{GCL}$ indicates Gouy-Chapman layer (GCL) capacitance [25], $C_{GCL}$= $((2Z_m^2 q n_E \varepsilon_{Water})/V_T)^{1/2}$, where m and $Z_m$ signify ions present in the electrolyte solution and the valence of $m^{th}$ ion respectively. In case of $SiO_2$, $pH_{Pzc}$ = 2 [4]. Now, the shifting of charge inside the channel generated by potential variations near dielectric/fluid intersection is stated as [4],

$$\Delta\sigma_H = -C_d\Delta\psi = -\frac{\varepsilon_0\varepsilon_d}{t_d}\Delta\psi \quad (2)$$

where $C_d$, Δψ, $\varepsilon_d$, and $t_d$ denote the capacitance of dielectric material, the variation in surface potential near dielectric/electrolyte interface, permittivity of the gate dielectric, and height of the dielectric correspondingly. After evaluating ψ from the expression (1), $\sigma_H$ can be computed and can be employed as intersection charge density ($D_{it}$) near the substrate-oxide junction to represent pH value [4] within the simulation. Fig. 2(d) illustrates the change of $D_{it}$ with pH value for 0.01 × PBS. A feasible fabrication flow [12], [26] for the

This article has been accepted for publication in IEEE Transactions on NanoBioscience. This is the author's version which has not been fully edited and content may change prior to final publication. Citation information: DOI 10.1109/TNB.2022.3202242



proposed model is specified in Fig. 3.

## IV. Device Performance and Optimization

### A. Impact of pH on $E_g$, Tunneling width ($T_W$), Optimal Electric Field ($E_{F,max}$) and $I_{DS}$-$V_{GS}$

The functioning of TFET devices is dependent on the energy band bending across the tunneling interface. $I_{DS}$ is proportional to BTBT probability (R) which is further influenced by an exponential deviation of forward gate voltage ($V_{FG}$) [4]. Moreover, $T_W$ near source/channel interface (SCI) is mostly adjusted by $D_{it}$ for $L_{un}$ = 50 nm [4]. Here, the pH values are presented in the sort of $D_{it}$.

While pH enhances commencing 1 to 10, the corresponding $D_{it}$ raises. As a result, $T_W$ reduces and R improves [4]. Fig. 4(a) depicts the variation of the energy band profile with a lateral distance along the channel at $V_{FG}$ = 0.6 V, back gate voltage ($V_{BG}$) = 0 V and drain-to-source voltage ($V_{DS}$) = 0.8 V [10]. The effect of pH on $T_W$ and $E_F$ is shown in Fig. 4(b)-(c). $T_W$ is greatest (least) for pH = 1 (10). Since, pH enhances from 1-10, $D_{it}$ raises and controllability of the gate upon channel region rises. Hence, $T_W$ is the lowest and $I_{DS}$ reaches to utmost value for pH = 10 as shown in Fig. 4(b). From Fig. 4(c), it is obvious that the $E_{F,max}$ near the SCI, below the electrolyte zone, changes proportionately with pH. Similarly, the proportional enhancement of $I_{DS}$ with pH is shown in Fig. 4(d). Fig. 4(d) elucidates an assessment of $I_{DS}$-$V_{GS}$ for different pH value. Here, the ON-state drain current ($I_{ON}$) enhances extensively by ~ three orders while pH varies from 1 (acidic) to 10 (basic). Furthermore, this is featured in the improved gate coupling regarding basic which offers enhanced $E_F$ (vertical) near the source-channel tunneling intersection as depicted in Fig. 4(c). This enhanced vertical $E_F$ directs to an important lessening in $T_W$ as illustrated in Fig. 4(a)-(b), thus, rising R and BTBT current run efficiently [27]. Hence, this

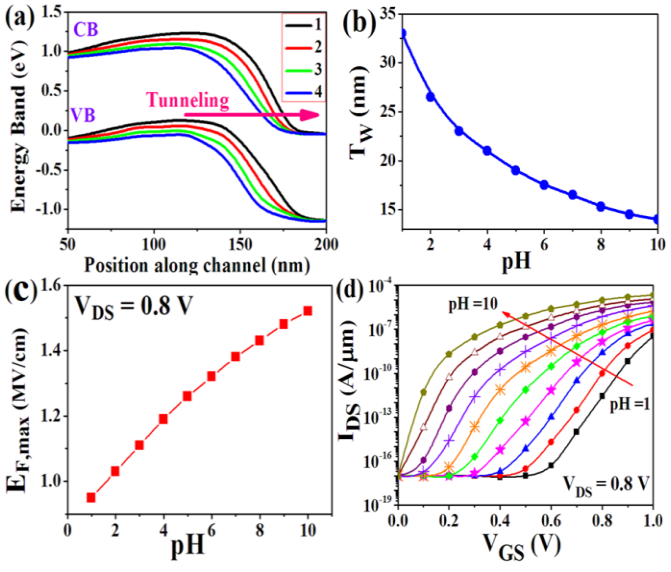


Fig. 4. Estimation of (a) $E_g$ vs. position along the channel with pH = 4, 6, 8, 10 of ionic solution as parameter (b) $T_W$ vs. pH of solvent (c) $E_{F,max}$ below the electrolyte zone vs. pH (d) $I_{DS}$-$V_{GS}$ features of the recommended design with variation of pH from 1 to 10 at $V_{DS}$ = 0.8 V, $T_{si}$ = 10 nm, and $L_{un}$ = 50 nm.

system outcome in a large enhances in $I_{ON}$ and attains to the peak value of ~ $2\times10^{-5}$ A/μm at pH = 10.

### B. Impact on $V_{TH}$

As the dielectric constant of the oxide layer (k) increases, the oxide capacitance of FG ($C_{ox} = k\phi_{ox}/T_{ox}$) enhances. Hence, $V_{TH}$ will reduce [10]. Moreover, as pH enhances from 1 to 10, $V_{TH}$ linearly diminishes. It is obvious that while pH is varied from 1 to 2 then the $V_{TH}$ shifts for $SiO_2$, $Si_3N_4$, $Al_2O_3$, and $HfO_2$ are 65.9, 69, 72.3, and 88.6 mV/pH, correspondingly, shown in Fig. 5(a). Fig. 5(b) describes the impact on $V_{TH}$ due to alteration of Ge mole fraction (x) in $Si_{1-x}Ge_x$ alloy [10]. As x enhances commencing 0.5 to 0.8, utmost current density ($J_{peak}$) improves [10] due to reduced zero bandgap energy ($E_g$) by following $E_g = (1.17-0.896x+0.396x^2-0.05)$ eV. Hence, $V_{TH}$ gradually decreases. Besides, as pH increases from 1 to 10, $V_{TH}$ linearly diminishes. It is apparent that while pH is varied from 1 to 2 then the $V_{TH}$ shifts for x = 0.5, 0.6, 0.7, and 0.8 are 65.9, 96.4, 92.1, and 114.2 mV/pH, correspondingly. So, for the best output, x is set as 0.5 [10] all through the simulation.

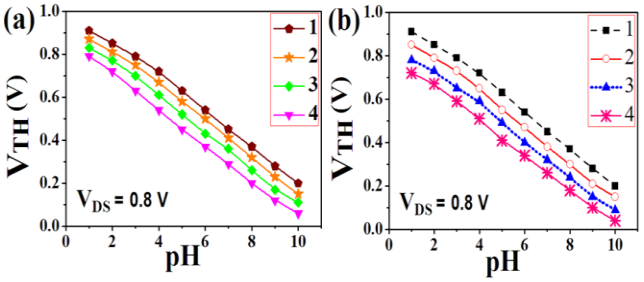


Fig. 5. Alteration of $V_{TH}$ regarding pH value with (a) FG oxide layers. Here, 1, 2, 3, and 4 denotes $SiO_2$, $Si_3N_4$, $Al_2O_3$, and $HfO_2$ layers. (b) Ge mole fraction as a parameter. Here, 1, 2, 3, and 4 signifies x= 0.5, 0.6, 0.7 and 0.8.

### C. Sensitivity Evaluation

#### 1) Impact of $I_{Ref}$ and $V_{Ref}$

Conventionally, $V_{TH}$ and $I_{DS}$ are assumed as the common metric in Bio-FET and the deviation of $V_{TH}$ or the ratio of $I_{DS}$ before and after the bioanalytes immobilization has been employed as the sensing metric [4]. Here, in TFET based pH sensor, the performance metrics akin to $S_v$ and $S_I$ are evaluated between two consecutive pH values [1], [4]. Hence, $I_{DS\ (pH\ =\ 1)}$ is assumed as the reference current ($I_{Ref}$). In Fig. 4(d), $V_{GS}$ for $I_{Ref}$ = $10^{-10}$ A, $10^{-11}$ A, and $10^{-12}$ A, is considered as a responsive potential ($V_{Resp}$) [4] and deviation in $V_{Resp} \approx \Delta V_{Resp}$ for pH variation is estimated respecting to pH = 1. In Fig. 6(a), for $I_{Ref}$ = $10^{-10}$ A, least (maximum) reading of $S_V$ is 60 mV/pH (100 mV/pH) while for $I_{Ref}$ = $10^{-11}$ A and $10^{-12}$ A, those values of $S_V$ are 70 mV/pH (100 mV/pH) and 80 mV/pH (100 mV/pH) respectively. Hence, $S_V$ > Nernstian limit. Now, $S_I = (I_{DS\ (pH\ >\ 1)} - I_{DS\ (pH\ =\ 1)})/I_{DS\ (pH\ =\ 1)}$ at a fixed $V_{GS} = V_{Ref}$ (reference voltage). Moreover, the correlation among $S_I$ and pH is revealed in Fig. 6(b) for the variation of $V_{Ref}$ = 0.6 V, 0.8 V and 1V respectively. Fig. 6(b) illustrates that the Bio-HTFET attains maximum $S_I$ of about $5\times10^{10}$, $3.7\times10^{6}$ and 628. $S_I$ improves with pH because of enhanced change in $I_{DS}$ related to two consecutive pH values. Moreover, $S_I$ > one decade/pH, is examined in TFET. The $S_V$ and $S_I$ are computed in this

This article has been accepted for publication in IEEE Transactions on NanoBioscience. This is the author's version which has not been fully edited and content may change prior to final publication. Citation information: DOI 10.1109/TNB.2022.3202242



article established on the perspective implemented in [28].

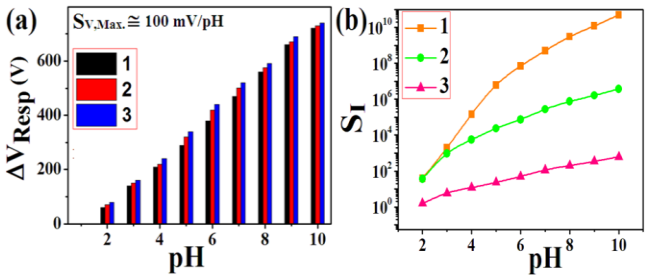


Fig. 6. Variation of (a) $\Delta V_{Resp}$ vs. pH for various $I_{Ref}$. Here, 1, 2, and 3 indicates $I_{Ref} = 10^{-10}$ A, $10^{-11}$ A, and $10^{-12}$ A (b) $S_I$ vs. pH for different $V_{FG} = V_{Ref}$. Here, 1, 2, and 3 indicates $V_{Ref} = 0.6$ V, 0.8 V, 1 V.

### 2) *Impact of $N_{CH}$, Ge mole fraction (x) and dielectric layer thickness ($T_{ox}$)*

The impact of $N_{CH} = 10^{14}/cm^3$, $10^{15}/cm^3$, and $10^{16}/cm^3$ are represented in Fig. 7(a)-(b). $N_{CH}$ does not vary $V_{Resp}$ and $S_V$ attains ~ 80-100 mV/pH for all $N_{CH}$ having $I_{Ref} = 10^{-11}$ A as shown in Fig. 7(a). Higher $N_{CH}$ provides a highly conductive channel region, however, $I_{DS}$ does not increase significantly [4]. So, $S_I$ becomes less at $N_{CH} = 10^{16}/cm^3$ compared to $N_{CH} = 10^{14}/cm^3$, and $10^{15}/cm^3$ as depicted in Fig. 7(b). Maximum $S_I$ ($S_{I,max}$) has been attained as $1.5 \times 10^{10}$ with $N_{CH} = 10^{14}/cm^3$ at $V_{Ref} = 0.6$ V. Generally, a good channel should not be doped with high $N_{CH}$. Hence, $N_{CH} = 10^{14}/cm^3$ is utilized here to achieve optimum biosensing performance. Fig. 8(a) illustrates the impact of x upon $S_{VTH}$ and $S_{ION}$, correspondingly. Here, $S_{VTH} = (V_{TH\,(pH>1)} - V_{TH\,(pH=1)})/V_{TH\,(pH=1)}$ and $S_{ION} = (I_{ON\,(pH>1)} - I_{ON\,(pH=1)})/I_{ON\,(pH=1)}$ at a fixed $V_{GS} = V_{Ref}$. When x increase commencing 0.5 to 0.8, Jpeak increases as $E_g$ decreases [10]. Hence, $S_{VTH}$ ($S_{ION}$) progressively reduces (enhances) and attains the maximum amount of deployment (increment) [10] of 35% ($3.5\times10^4$%) due to the BTBT event. Fig. 8(b) reveals the impacts of $T_{ox}$ deviations upon $S_{VTH}$ and $S_{ION}$, correspondingly. While $T_{ox}$ enhances, the effect of localized $D_{it}$ upon $V_{TH}$ becomes further remarkable as flat band potential ($V_{FB}$) changes by ensuing $V_{FB} = V_{FB0} + qT_{OX}D_{it}/C\varepsilon_{ox}$, where $V_{FB0}$ specifies the flat-band voltage without $D_{it}$ [10]. Thus, 0.1 μA/μm current is realized later, and so, ($I_{ON}$) lessens [10]. It is viewed that $S_{VTH}$ ($S_{ION}$) achieves the highest sensitivity enrichment (reduction) by an extent of $1.25\times10^2$% (94.3%) for the proposed model with $T_{ox} = 5$ nm. Hence, it has been observed that the intersection point of $S_{VTH}$ and $S_{ION}$ contour might be the better option in terms of sensitivity.

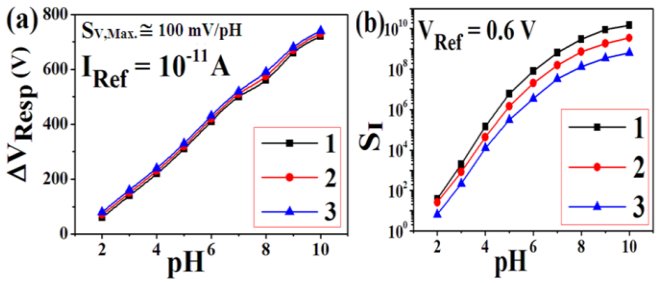


Fig. 7. Variations of (a) $\Delta V_{Resp}$ with pH of electrolyte at $I_{Ref} = 10^{-11}$ A (b) $S_I$ vs. pH at $V_{Ref} = 0.6$ V. Here, 1, 2, and 3 symbolizes $N_{CH} = 10^{14}/cm^3$, $10^{15}/cm^3$, and $10^{16}/cm^3$.

Thus, $T_{ox} = 3.85$ nm ≈ 4 nm is assumed throughout the simulation work to achieve best performance of the proposed Bio-TFET.

### *D. Limit of Detection (LOD) Evaluation*

The minimal charge recognition limit [22] relies on (i) geometry of the configuration (ii) electrolytic concentration (iii) configuration and features of the bioanalytes (iv) functionalization of the surface and (v) biasing of the device (sub-$V_{TH}$) is preferable [22]. The effective capacitance, $C_{eff}$ is the series combination of $C_{GCL}$ and $C_{STERN}$, given as, $C_{eff} = (C_{GCL} \times C_{STERN})/(C_{GCL} + C_{STERN})$. Hence, the minimal detected charge for lesser ionic concentration, $Q_{BIO,\,Min.}$ ($C_{eff} \times \Delta\psi_{Min.}$) = $834.2 \times 10^{-15}$ C and therefore simulation results illustrate that $\Delta\psi_{Min.}$ is 7.2 mV. Considering, APTES (k ≈ 3.57; molecular weight ($M_W$) = 221.37 Da) [27], nearly the limit of detection (LOD) = 12 aM is probable within an array of 10 biosensors having underlapped length ($L_{un}$) ≈ 50 nm and electrolyte thickness ($T_{Electrolyte}$) ≈ 37 nm. Yet, tinier bioanalytes like proteins (lesser than 10 nm) in the range of aM ~ fM ionic concentration having superior sensitivity can be realized.

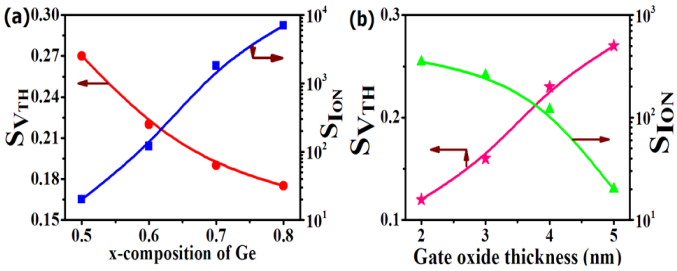


Fig. 8. Assessment of sensitivity with the variation of (a) molar fraction (x) of Ge (b) $T_{ox}$ at $V_{DS} = 0.8$ V.

### *E. Assessment with State-of-the-Art Literature*

In Table-I, sensitivities extracted from the state-of-the-art literature with the different structural, and doping environments. The outcomes of the proposed underlapped TFET have been assessed with the inversion mode (IM) configurations [1]-[3], [29]-[32] to illustrate the superior presentation of Bio-TFET. Employing the BTBT phenomenon in the TFET, maximum $S_V$ attains ≈ 100 mV/pH > Nernstian limit. Hence, the obtained $S_V$ employing TFET is significantly superior to the $S_V$ value achieved for the IM device. This superior $S_V$ enhances the efficacy of Bio-TFET, yet for the situation where lesser samples of bio-analytes are offered. Thus, Bio-TFET can be a hopeful contender as a pH sensor.

## V. Impact Of Temperature On Device Performance

In an Electrolyte biosensor, the $V_{TH}$ of the pH sensors depends on the pH of the buffer solvent and temperature. pH is also a function of the temperature. So, it is indispensable to assess the changes in the sensing performances due to temperatures variations [5]-[6]. Temperature can sway the electrolyte-oxide interface charges and surface dipole potential of the solvent. Moreover, ψ has a strong reliance on temperature [5]-[6]. Hence, $V_{TH}$ can be written as,

$$V_{TH} = \varphi_{lj} - \psi + \chi_{el} + \varphi_f - (\xi_e + 0.5E_g)q^{-1} - \left(Q_{\text{int}} + Q_{dep}\right)\left(C_{in}\right)^{-1} \quad (3)$$

where, the factors are, $\phi_{lj}$: potential variation at liquid interface; $\chi_{el}$: Surface dipole potential of the solvent; $\phi_f$: Fermi potential of semiconductor; $q$: electronic charge; $\xi_e$: affinity of electrons in semiconductor; $Q_{int}$: correspondent insulator-silicon intersection charge/unit area; $Q_{dep}$: the depletion charge/unit area of silicon at $V_{TH}$; $C_{in}$: insulator capacitance/ unit area.

TABLE I: BENCHMARKING OF SENSITIVITY PROFILE OF REPORTED FET BASED PH SENSOR

| FET Based pH sensor | Approx. Voltage Sensitivity (mV/pH) |
|---|---|
| JL-SOI-ISFET [1] | 63.4 |
| Fully depleted (FD) SOI-ISFET [2] | 47.9 |
| Si-ISFET [3] | 59 |
| Extended-gate ISFET with ALD $Al_2O_3$ growth [29] | 40 |
| Double-gate (DG) Si-Nanowire (NW) TFET [30] | 68 |
| Si-NW TFET [31] | 56.4 |
| DG-FET [32] | 60 |
| Underlapped electrolyte Bio-HTFET (Our Work) | 100 |

### *A. Impact of Oxide-Electrolyte Intersection terms*

$\chi_{el}$ at oxide-electrolyte intersection strongly rely on temperature. Moreover, it depends on the arrangement of the polarity of $H_2O$ molecules near the oxide surface. Thermal disturbance interrupts this arrangement. Besides the ionic strength of buffer solution ($I_B$) affects $\chi_{el}$ [5]-[6], as given by,

$$\chi_{el}(T, I_B) = 50(1 - e^{-0.86\,pI_B}) \times [1 - 0.008(T - 298.2)]\ mV \quad (4)$$

where, $pI_B = -\log(I_B)$. In equation (3), $\psi$ is the most significant term for the investigation of temperature reliance. Its dependency over pH as well as temperature, is developed with SB and EDL model [1]. $\psi$ is specified by [4], $\psi = \sigma_H/C_{eff}$.

### *B. Impact of temperature on pH buffer*

pH of hydrogen ion buffer changes with temperature (T) as per the relation stated as [7],

$$pH = M/T + N + O \times T + P \times T^2 \quad (5)$$

where M, N, O, and P are the constants and is dependable on the nature of solvent utilized. Here, M = 2558, N = -4.3, O = 0.02, P = 0 are considered as practical values for pH buffer [5]. Fig. 9(a) depicts the reduction of pH with temperature. Since, an increase in temperature enhances molecular vibrations, the recognizable [H+] is also enhanced owing to a diminished trend of composing hydrogen bonds.

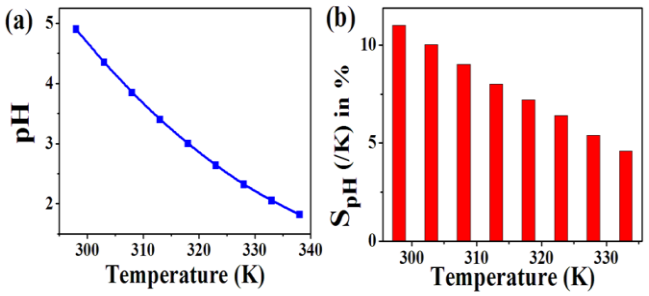


Fig. 9. Variations of(a) pH of hydrogen ion buffer and (b) $S_{pH}$ (/K) in % with T(K).

Now, the sensing parameter, $S_{pH}$ ($\Delta pH/\Delta T$) is plotted with respect to temperature (K) as depicted in Fig. 9(b). Here, $S_{pH}$ also diminishes with temperature.

### *C. Impact of temperature on $I_{DS}$*

Temperature-dependent semiconductor factors akin to $\phi_f$, $E_g$, $n_i$, $N_C$, and $N_V$ influences $V_{TH}$ and $I_{DS}$ and are expressed as,

$$\phi_f = V_T \times \ln(N_a/n_i)\ V \quad (6)$$

$$E_g(T) = [E_g(0) - ((g \times T^2)/(T + h))]\ eV \quad (7)$$

$$\xi_e(T) = \xi_e(0) + (1/2) \times ((g \times T^2)/(T + h)) \quad (8)$$

where $E_g(0)$, $\xi_e$ and $N_a$ denote $E_g$ at T= 0 K for semiconductor, electron affinity, the impurity concentration of acceptor ions, g and h are the experimental factors alter with T. For TFET, T-dependency appears from $E_g$ and the equation of BTBT current is given as [33]:

$$I_{DS} = U \frac{|E|^2}{E_g^{1/2}} \exp\left(-\frac{VE_g^{3/2}}{|E|}\right) \quad (9)$$

where U and V denote the default material-reliant factors described in Silvaco ATLAS [20]. Hence, with temperature, $E_g$ diminishes and $I_{DS}$ enhances. The effect of temperature is less (large) in the ON (OFF)-state due to the domination of BTBT (SRH) model, which is impotently (greatly) reliant on T [33]. Here, Table II shows the temperature effect on transfer characteristics of HTFET. Subthreshold swing (SS), which is defined as the switching ability, is also a function of temperature. Here, SS rises with temperature.

### *D. Impact of temperature on $\Delta V_{Resp}$ and $S_I$*

Fig. 10(a)-(b) illustrates $\Delta V_{Resp}$ and $S_I$ variations with pH for back gate work-function ($\varphi_{BG}$) = 4.2 eV, 4.7 eV and 5.1 eV having $V_{BG}$ = 0 V. Here, $\varphi_{BG}$ = 0 eV is considered as initial state. In Fig. 10(a), $\Delta V_{Resp}$ demonstrates the slight reliance on $\varphi_{BG}$ and roughly offers $S_V \approx$ 80-100 mV/pH for all pH value at $I_{Ref} = 10^{-12}$ A. Moreover, Fig. 10(a) demonstrates high linearity for $\varphi_{BG}$ variations. Fig. 10(b) explains that $S_I$ varies significantly with $\varphi_{BG}$ as assessed by $S_V$ [4]. For the higher $\varphi_{BG}$, $T_W$ enhances and the controlling capability of the gate near SCI reduces and consequently $I_{DS}$ decreases as shown in Fig. 10(b). Hence, $S_I$ attains a maximum value of $3\times10^{10}$ for $\varphi_{BG}$ = 4.2 eV at $V_{Ref}$ = 0.6 V. Fig. 10(c)-(d) highlights the temperature effect on $\Delta V_{Resp}$ and $S_I$. With temperature, a significant change of $I_{DS}$ in sub-threshold regime is observed due to the dominance of SRH model. Hence, $\Delta V_{Resp}$ at $I_{Ref} = 10^{-12}$ A shows considerable change in $S_V$ and $S_I$. It has been observed that $\Delta V_{Resp}$ and $S_I$ reduces as temperature increases. This is owing to pH value reduction with the progress of temperature as illustrated in Fig. 9(a).

### *E. Assessment of $S_T^{V_{TH}}$ of state-of-the-art literature*

Instability in the threshold voltage ($V_{TH}$) is defined as drift [5]. In a pH sensor, the amount of inversion charge ($Q_{inv}$) accumulated within the semiconductor at a certain $V_{GS}$ alters with time (t) gradually, directing to a uniform temporal variation in $V_{TH}$ [5]-[6], [34] and is expressed as,

$$Q_{inv} = C_{in} \times (V_{GS} - V_{TH}) \quad (10)$$

This article has been accepted for publication in IEEE Transactions on NanoBioscience. This is the author's version which has not been fully edited and content may change prior to final publication. Citation information: DOI 10.1109/TNB.2022.3202242



Actually, chemical operations that occur near the sensing layer surface, reduce the resultant insulator capacitance, $C_{in}$, for which $V_{TH}$ directs a temporal variation [5]-[6], [34]. This $Q_{inv}$ is generated while $V_{GS} > V_{TH}$ [5]. Hence, the drift in $V_{GS}$ is responsible for the drift in $V_{TH}$. The drift in $V_{GS}$ [5]-[6] is,

$$\Delta V_{GS}(t) = -(Q_{dep} + Q_{int} + Q_{inv}) \times \left(\frac{\varepsilon_{dl} - \varepsilon_{sf}}{\varepsilon_{dl} \times \varepsilon_{sf}}\right) \times x_{sf}(t) \quad (11)$$

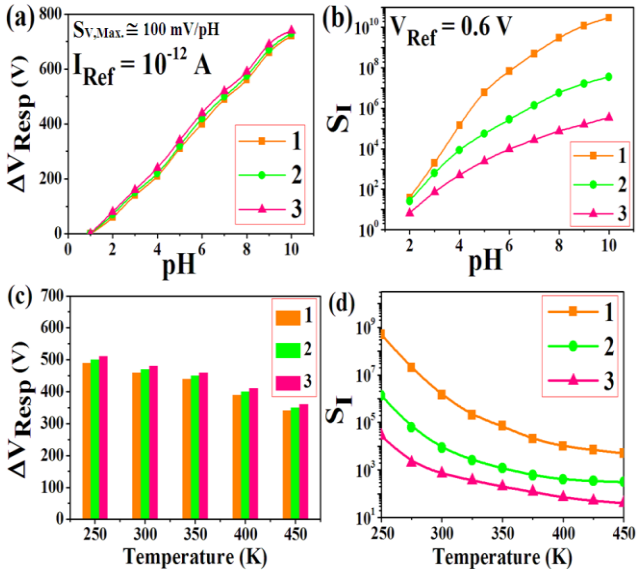


Fig. 10. Variation of (a) $\Delta V_{Resp}$ vs. pH at $I_{Ref} = 10^{-12}$ A (b) $S_I$ vs. pH at $V_{Ref} = 0.6$ V (c) $\Delta V_{Resp}$ vs. temperature (K) at $I_{Ref} = 10^{-12}$ A and (d) $S_I$ vs. temperature (K) at $V_{Ref} = 0.6$ V. Here, 1, 2, and 3 symbolizes $\varphi_{BG} = 4.2$ eV, 4.7 eV and 5.1 eV.

where, $x_{sf}$ (t), $\varepsilon_{dl}$ and $\varepsilon_{sf}$ denote height of the revised surface film (RSF) at any instant 't', permittivity of dielectric sensing layer and RSF correspondingly. Moreover, temperature dependent parameter, $Q_{dep}$ is evaluated using the following equation as [5]-[6], $Q_{dep} = -2 \times \sqrt{\varepsilon_s q N_a \phi_f}$ C/cm$^2$ (12)

Here $\varepsilon_s$ denotes the substrate permittivity and $\phi_f = V_T \times \ln(N_a/n_i)$ V; $V_T$, $N_a$ and $n_i$ denote the thermal potential, impurity concentration of acceptor ions and intrinsic carrier concentration respectively. With the variation of temperature, temporal drift parameter, $Q_{dep}$ changes and hence $V_{TH}$ varies. Fig. 11 demonstrates the deviation in $V_{TH}$ with temperature.

Cryopreservation biotechnology (-150°C to -273°C) spotlights over conservation of cells, tissues that have wide utilizes in the territories of medicine, agricultural science and aquafarming [33]. The temperature reliance of electrolyte biosensors based on ISFET [1], [3], [24], [28], TFET [4], and HTFET (our work) at pH = 7 are examined here. In this context, we assume the impact of temperature on $V_{TH}$ ($S_T^{V_{TH}}$) as a sensing factor. It is obvious, from Table III that while temperature changes from 75 K to 425 K with an increment of 50 K then $V_{TH}$ changes in a sluggish manner for TFET based electrolyte sensor and attains the maximum $S_T^{V_{TH}}$ value of ≈ 0.7 mV/K. While others reported published work mainly based on ISFET [3], [5], [24], [28], and TFET [4] attain maximum $S_T^{V_{TH}}$ value of ≈ 1.6 mV/K, 1.8 mV/K, 1.6 mV/K, 2 mV/K, and1.2 mV/K respectively. Hence, the assessment related to state-of-the-art literature exposes that HTFET is more immune to temperature variation as compared to ISFET and TFET and exhibits positive-temperature coefficient for the variety regarded as.

TABLE II: TEMPERATURE-RELIANCE OF $I_{DS}$-$V_{GS}$ FEATURES

| T in K | Industrial Sector/Process | $I_{ON}$ (A/m) | $I_{OFF}$ (A/μm) | $I_{ON}/I_{OFF}$ | SS (mV/dec) |
|---|---|---|---|---|---|
| 253 | Medical/Saliva preservation | 221 | $1.04 \times 10^{-17}$ | $2.2 \times 10^{12}$ | 6.8 |
| 313 | Textile/washing | 292 | $5.32 \times 10^{-16}$ | $5.7 \times 10^{10}$ | 11.5 |
| 353 | Food/drying | 335 | $3.67 \times 10^{-14}$ | $9.12 \times 10^{8}$ | 17.3 |
| 405 | Food/ steam-sterilizing | 383 | $4.31 \times 10^{-12}$ | $8.9 \times 10^{6}$ | 28.2 |
| 453 | Healthcare/dry heat sterilizing | 427 | $3.26 \times 10^{-11}$ | $1.3 \times 10^{6}$ | 39.4 |

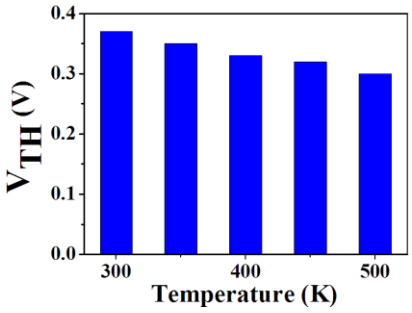


Fig. 11. Impact of temperature on $V_{TH}$ (V).

TABLE III: TEMPERATURE-DEPENDENCE OF ELECTROLYTE BIOSENSOR

| T in K | $S_T^{V_{TH}}$ (mV/K) at pH = 7 | | | | | |
|---|---|---|---|---|---|---|
| | [1] | [3] | [24] | [28] | [4] | This Work |
| 75 | 1.4 | 1.8 | 1.6 | 1.8 | 1.2 | 0.7 |
| 125 | 1.6 | 1.4 | 1.4 | 2 | 1 | 0.6 |
| 175 | 1.4 | 1.2 | 1.2 | 1.6 | 1 | 0.5 |
| 225 | 1.6 | 1.6 | 1.2 | 1.8 | 1.2 | 0.5 |
| 275 | 1.2 | 1.8 | 1.6 | 1.4 | 1 | 0.7 |
| 325 | 1.2 | 1.2 | 1.6 | 1.4 | 1.1 | 0.6 |
| 375 | 1.6 | 1.2 | 1.4 | 1.2 | 0.8 | 0.5 |
| 425 | 1.4 | 1.6 | 1.2 | 1.6 | 1 | 0.7 |

## V. CONCLUSION

An underlapped hetero-structure electrolyte Bio-TFET has been recommended here to study the pH sensing. The electrolyte section is illustrated by adjusting the features of an undoped semiconductor material. The effects of pH on the various electrical features have been inspected. The impact of shielding is included by enhancing $T_{BIO}$ among CS film and the gate dielectric layer of the sensor. Utilizing the BTBT event in TFET, $S_V$ accomplishes ≈ 100 mV/pH that is greater than the Nernstian limit (59 mV/pH) and $S_I$ enhances almost an order 10 per pH change. The impact of temperature on pH buffer solution, $I_{DS}$, temporal drift parameters and sensitivity factors of the proposed sensor is scrutinized properly. Lastly, a temperature-immunity feature of proposed HTFET based pH sensor is highlighted by comparing $S_T^{V_{TH}}$ parameter with state-of-the-art literature. Thus, the suggested pH sensor can be employed as an exceptional alternate for the succeeding

generation of biosensing purposes.

## REFERENCES


[1] Ajay, R. Narang, M. Saxena, and M. Gupta, "Analytical Model of pH sensing Characteristics of Junctionless Silicon on Insulator ISFET," *IEEE Trans. Electron Devices*, vol. 64, no. 4, pp. 1742–1750, Apr. 2017. doi: 10.1109/TED.2017.2668520.

[2] H. J. Jang and W.-J. Cho, "Fabrication of high-performance fully depleted silicon-on-insulator based dual-gate ion-sensitive field-effect transistor beyond the Nernstian limit," *Appl. Phys. Lett.*, vol. 100, no. 7, pp. 073701-1–073701-4, Feb. 2012.doi: 10.1063/1.3685497.

[3] A. Bandiziol, P. Palestri, F. Pittino, D. Esseni, and L. Selmi, "A TCAD based methodology to model the site-binding charge at ISFET/electrolyte interfaces," *IEEE Trans. Electron Devices*, vol. 62, no. 10, pp. 3379–3386, Oct. 2015. doi: 10.1109/TED.2015.2464251.

[4] P. Dwivedi, R. Singh, and Y. S. Chauhan, "Crossing the Nernst Limit (59 mV/pH) of Sensitivity Through Tunneling Transistor-Based Biosensor," *IEEE Sens. J.*, vol. 21, no. 3, pp. 3233-3240, sept. 2020. doi: 10.1109/JSEN.2020.3025975.

[5] S. Sinha, R. Bhardwaj, N. Sahud, H. Ahujad, R. Sharma, R. Mukhiya, "Temperature and temporal drift compensation for $Al_2O_3$-gate ISFET-based pH sensor using machine learning techniques," *Microelectro. J.*, vol. 97, pp. 104710, Feb. 2020. doi: 10.1016/j.mejo.2020.104710.

[6] R. Bhardwaj, S. Sinha, N. Sahu, S. Majumder, P. Narang, R. Mukhiya, "Modeling and simulation of temperature drift for ISFET-based pH sensor and its compensation through machine learning techniques," *Int. J. Circ. Theor. Appl.*, vol. 47, no. 6, pp. 954–970, Jan. 2019.doi: 10.1002/cta.2618.

[7] J. Y. Kim *et al.*, "An underlap channel-embedded field-effect transistor for biosensor application in watery and dry environment," *IEEE Trans. Nanotechnol.*, vol. 11, no. 2, pp. 390–394, Mar. 2012. doi: 10.1109/TNANO.2011.2175006.

[8] G. Wadhwa and B. Raj, "Parametric variation analysis of symmetric double gate charge plasma JLTFET for biosensor application," *IEEE Sensors J.*, vol. 18, no. 15, pp. 6070–6077, Aug. 2018, doi: 10.1109/JSEN.2018.2846409.

[9] G. Wadhwa and B. Raj, "Design, simulation and performance analysis of JLTFET biosensor for high sensitivity," *IEEE Trans. Nanotechnol.*, vol. 18, pp. 567–574, May 2019, doi: 10.1109/TNANO.2019.2918192.

[10] A. Bhattacharyya, M. Chanda, and D. De, "Performance Assessment of New Dual-Pocket Vertical Heterostructure Tunnel FET-Based Biosensor Considering Steric Hindrance Issue," *IEEE Trans. Electron Devices*, vol. 66, no. 9, pp. 3988-3993, Sep. 2019. doi: 10.1109/TED.2019.2928850.

[11] A. Bhattacharyya, M. Chanda, and D. De, "Analysis of Noise-Immune Dopingless Heterojunction Bio-TFET Considering Partial Hybridization Issue," *IEEE Trans. Nanotechnol.*, vol. 19, pp. 769–777, Oct. 2020. doi: 10.1109/TNANO.2020.3033966. (Early Access)

[12] P. Dwivedi and A. Kranti, "Dielectric modulated biosensor architecture: tunneling or accumulation based transistor?" *IEEE Sens. J.*, vol. 18, no. 8, pp. 3228-3235, 2018. doi: 10.1109/JSEN.2018.2808948.

[13] S. Uno , M. Iio, H. Ozawa, and K. Nakazato, "Full Three-Dimensional Simulation of Ion-Sensitive Field-Effect Transistor Flatband Voltage Shifts Due to DNA Immobilization and Hybridization," *Jpn. J. Appl. Phys*, vol. 49, no. 1, Jan. 2010. doi: 10.1143/JJAP.49.01AG07.

[14] B. M. Lowe, K. Sun, I. Zeimpekis, C.-K. Skylaris, and N. G. Green, "Field-effect sensors–from pH sensing to biosensing: Sensitivity enhancement using streptavidin–biotin as a model system," *Analyst*, vol. 142, no. 22, pp. 4173–4200, 2017, doi: 10.1039/ C7AN00455A.

[15] E. L. Sciuto, C. Bongiorno, A. Scandurra, S. Petralia, T. Cosentino, S. Conoci, F. Sinatra and S. Libertino, "Functionalization of Bulk SiO2 Surface with Biomolecules for Sensing Applications: Structural and Functional Characterizations," *Chemosensors*, vol. 6, no. 4, pp. 59, Nov. 2018, doi:10.3390/chemosensors6040059.

[16] A. Bhattacharyya, M. Chanda, and D. De, "Analysis of partial hybridization and probe positioning on sensitivity of a dielectric modulated junctionless label free biosensor," *IEEE Trans. Nanotechnol.*, vol. 19, pp. 719–727, Sep. 2020, doi: 10.1109/TNANO. 2020.3025544.

[17] L. Vroman and A. L. Adams, "Findings with the recording ellipsometer suggesting rapid exchange of specific plasma proteins at liquid~solid interfaces," *Surface Science*, vol. 16, pp. 438-446, Aug. 1969, doi:10.1016/0039-6028(69)90037-5.

[18] W. Muangsuwan, C. Promptmas, W. Jeamsaksiri, and W. Bunjongpru, *et al*., " Development of an immunoFET biosensor for the detection of biotinylated PCR product," *Heliyon*, vol. 2, no. 10, pp. e00188, Oct. 2016, doi: 10.1016/j.heliyon.2016.e00188.

[19] S. Choi, I. Park, Z. Hao, H.-Y. N. Holman, and A. P. Pisano, ''Quantitative studies of long-term stable, top-down fabricated silicon nanowire pH sensors,'' *Appl. Phys. A*, vol. 107, no. 2, pp. 421–428, May 2012, doi: 10.1007/s00339-011-6754-9.

[20] *ATLAS Device Simulation Software*, Silvaco Int., Santa Clara, CA, USA, 2016.

[21] S. H. Kim, H. Kam, C. Hu, and T. J. K. Liu, "Germanium-source tunnel field effect transistors with record high $I_{ON}/I_{OFF}$," in *Proc. Int. Symp. VLSI Tech., Dig.*, Jun. 2009, pp. 178–179.

[22] X. P. A. Gao, G. Zheng, and C.M. Lieber, "Subthreshold Regime has the Optimal Sensitivity for Nanowire FET Biosensors", *NANO letters*, vol. 10, no. 2, pp. 547-552, Dec. 2009, doi: 10.1021/nl9034219.

[23] N. Shafi, A. M. Bhat, J. S. Parmar, C. Sahu and C. Periasamy, "Analytical modeling of surface potential and figure of merit computation for planar junctionless pH sensing biofet", *IEEE Trans. Nanotechnol.*, vol. 20, pp. 534-542, June, 2021, doi: 10.1109/TNANO.2021.3089717.

[24] Ajay, R. Narang, M. Saxena, and M. Gupta, "Novel junctionless electrolyte-insulator-semiconductor field-effect transistor (JL EISFET) and its application as pH/biosensor," *Microsyst. Technol.*, vol. 23, no. 8, pp. 3149–3159, June 2016. doi: 10.1007/s00542-016-3013-1.

[25] D. Landheer, G. Aers, W. R. McKinnon, M. J. Deen, and J. C. Ranuarez, "Model for the field effect from layers of biological macromolecules on the gates of metal-oxide-semiconductor transistors," *J. Appl. Phys.*,vol. 98, no. 4, pp. 044701-1–044701-15, Aug. 2005. doi: 10.1063/1.2008354.

[26] H. Im, X. J. Huang, B. Gu, and Y. K. Choi, "A dielectric-modulated field-effect transistor for biosensing," *Nature Nanotechnol.*, vol. 2, no. 7, pp. 430–434, Jun. 2007, doi: 10.1038/nnano.2007.180.

[27] A. Bhattacharyya, D. De, and M. Chanda, "Sensitivity Measurement for Bio-TFET Considering Repulsive Steric Effects With Better Accuracy," *IEEE Trans. Nanotechnol*, vol.21, pp. 100-109, Jan. 2022, doi: 10.1109/TNANO. 2022. 3148922. (Early access)

[28] N. Liu, Y. H. Liu, P. Feng, L. Q. Zhu, Y. Shi, and Q. Wan, "Enhancing the pH sensitivity by laterally synergic modulation in dual-gate electric-double-layer transistors," *Appl. Phys. Lett.*, vol. 106, no. 7, pp. 073507, Feb. 2015. doi: 10.1063/1.4913445.

[29] K. B. Parizi, A. J. Yeh, A. S. Y. Poon and H. S. P. Wong, "Exceeding Nernst limit (59mV/pH): CMOS-based pH sensor for autonomous applications," 2012 International Electron Devices Meeting, 2012, pp. 24.7.1-24.7.4, doi: 10.1109/IEDM.2012.6479098.

[30] J.-H. Ahn, J.-Y. Kim, M.-L. Seol, *et al.*, "A pH sensor with a double-gate silicon nanowire field-effect transistor," *Appl. Phys. Lett.*, vol. 102, no. 8, p. 083701, Feb. 2013, doi: 10.1063/1.4793655.

[31] S. Chen, J. G. Bomer, E. T. Carlen, and A. van den Berg, "$Al_2O_3$/Silicon NanoISFET with Near Ideal Nernstian Response," *Nano Lett.*, vol. 11, no. 6, pp. 2334–2341, Jun. 2011, doi: 10.1021/nl200623n.

[32] J. Go, P. R. Nair, B. Reddy, B. Dorvel, R. Bashir, and M. A. Alam, "Beating the Nernst limit of 59mV/pH with double-gated nano-scale field-effect transistors and its applications to ultra-sensitive DNA biosensors," in *2010 International Electron Devices Meeting*, Dec. 2010, vol. 2, pp. 8.7.1-8.7.4, doi: 10.1109/IEDM.2010.5703325.

[33] R. Narang, M. Saxena, R. S. Gupta, and M. Gupta, "Impact of temperature variations on the device and circuit performance of tunnel FET: A simulation study," *IEEE Trans. Nanotechnol.*, vol. 12, no. 6, pp. 951–957, Nov. 2013. doi: 10.1109/TNANO.2013.2276401.

[34] A. Elyasi, M. Fouladian, and S. Jamasb, " Counteracting threshold-voltage drift in ion-selective field effect transistors (ISFETs) using threshold-setting ion implantation," *IEEE J. Electron Devices Soc.*, vol. 6, pp. 747–754, June 2018. doi: 10.1109/JEDS.2018.2847740.